

# Mojito: Motion Trajectory and Intensity Control for Video Generation

Xuehai He<sup>1</sup>    Shuohang Wang<sup>2</sup>    Jianwei Yang<sup>2</sup>    Xiaoxia Wu<sup>2</sup>    Yiping Wang<sup>3</sup>  
 Kuan Wang<sup>4</sup>    Zheng Zhan<sup>5</sup>    Olatunji Ruwase<sup>2</sup>    Yelong Shen<sup>2</sup>    Xin Eric Wang<sup>1</sup>

<sup>1</sup>University of California, Santa Cruz    <sup>2</sup>Microsoft    <sup>3</sup>University of Washington

<sup>4</sup>Georgia Institute of Technology    <sup>5</sup>Northeastern University

{xhe89, xwang366}@ucsc.edu,    {yelong.shen, olruwase, shuohang.wang}@microsoft.com

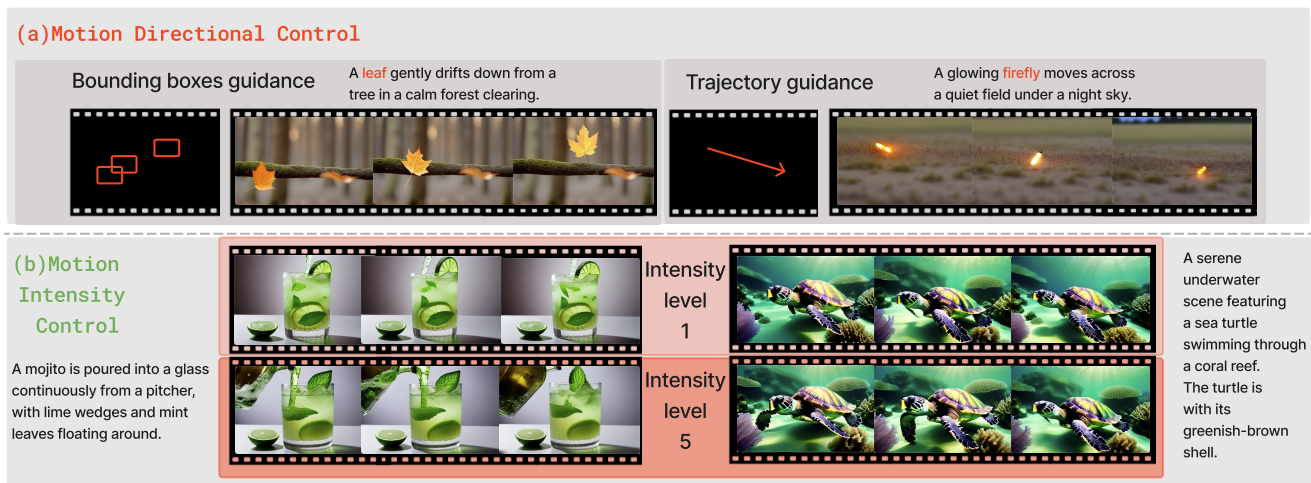


Figure 1. Mojito generates videos that accurately follow specified directions, locations, and trajectories, while adapting to varying input motion intensities. (a) **Motion Directional Control**: Mojito can follow input bounding box trajectories for an object (**leaf**, **firefly**) over time. (b) **Motion Intensity Control**: increasing input motion intensity level results in a corresponding increase in motion, turning a relatively static scene into one with dynamic movement. Project page: <https://sites.google.com/view/mojito-video>

## Abstract

Recent advancements in diffusion models have shown great promise in producing high-quality video content. However, efficiently training diffusion models capable of integrating directional guidance and controllable motion intensity remains a challenging and under-explored area. This paper introduces Mojito, a diffusion model that incorporates both **Motion trajectory and intensity control** for text to video generation. Specifically, Mojito features a **Directional Motion Control** module that leverages cross-attention to efficiently direct the generated object’s motion without additional training, alongside a **Motion Intensity Modulator** that uses optical flow maps generated from videos to guide varying levels of motion intensity. Extensive experiments demonstrate Mojito’s effectiveness in achieving precise trajectory and intensity control with high computational efficiency, generating motion patterns that closely match spec-

ified directions and intensities, providing realistic dynamics that align well with natural motion in real-world scenarios.

## 1. Introduction

Video generation, and specifically text-to-video (T2V) generation [1, 14, 23, 40, 45, 47, 52], aims to produce diverse, high-quality videos that match given text prompts. Unlike image generation [3, 28, 31, 34, 37, 49], which focuses on generating a single static frame, video generation must ensure consistent and fluid motion across a sequence of frames. However, existing models struggle to provide flexible, controllable motion effects in response to user prompts, particularly when handling specific motion directions or varying levels of motion intensity. Moreover, these models often fall short in generating videos with large motion am-

plitudes or adaptable motion strengths that align with user intent. Figure 1 illustrates these challenges, which Mojito effectively addresses through both an efficient, training-free method for direction control and a novel training-based approach for motion intensity modulation.

Achieving precise control over both motion direction and intensity in video generation poses great challenges. First, capturing relative motion data is inherently complex in real-world videos due to the simultaneous movements of both cameras and objects; Second, there is a lack of large-scale, annotated datasets specifically for motion direction and intensity. Existing video datasets rarely include detailed labels for motion dynamics, and obtaining human annotations for these subtle aspects is both costly and labor-intensive; Third, training models with such detailed annotations would demand substantial computational resources.

To address these challenges, we present Mojito, the first diffusion model for text-to-video generation that simultaneously integrates text-based prompts with flexible motion controls, allowing for the precise modulation of both motion direction and intensity. To achieve this, Mojito introduces two novel modules on top of the trained backbone: (1) the *Directional Motion Control* (DMC) module, which adjusts motion direction through cross-attention, aligning object trajectories with specified paths; and (2) the *Motion Intensity Modulator* (MIM) module, which encodes arbitrary motion intensities as features and integrates them seamlessly into the diffusion framework. Additionally, we explore an alternative by training a global motion intensity embedding layer as a conditional input to further enhance control over motion intensity.

Our contributions are summarized as follows:

- We introduce Mojito, a diffusion-based transformer model for text-to-video generation with integrated trajectory/direction guidance and motion intensity control.
- We introduce a training-free, test-time directional guidance method that enables text-to-video generation with specified trajectories or directions.
- We develop a training-based method for motion-guided generation that allows precise control over motion intensity to match user-defined motion levels.
- We demonstrate that Mojito not only generates high-quality video content comparable to state-of-the-art models but also provides effective and efficient motion control. Through ablations, we provide insights into designing efficient, motion-controllable video generation techniques, emphasizing essential factors for advancing future motion-augmented video generative models.

## 2. Related Works

### 2.1. Diffusion-based Text to Video Generation

With the rapid development of generative models, particularly diffusion models, numerous breakthroughs have been achieved in fields such as image generation [34] and video generation [5, 14, 23, 40, 45, 47, 52]. Regarding text-to-video (T2V) models, Make-A-Video [38], Imagen Video [36] are cascaded models, while most other works, such as LVDM [14], ModelScope [41], and Align your Latents [2], are Stable Diffusion-based models. They extend the SD framework to videos by incorporating temporal layers to ensure temporal consistency among frames and the spatial parameters are inherited from the pretrained SD UNet. Our model follows a similar architectural approach, using spatial transformers for spatial information processing and accepting directional control, and incorporating temporal transformers to manage temporal coherence.

### 2.2. Controllable Text-to-Visual Generation

Recent advancements in text-to-visual generation have enabled more precise and stable control over generated outputs. In image generation, several models [17, 27, 29, 51] have been developed to enhance control by leveraging semantic guidance from text prompts alongside various structural conditions. Some approaches utilize attention maps and bounding boxes to manage image layouts, enabling generation based on regional specifications [4, 6, 11, 13, 24, 46]. Mo et al. [26] presents a training-free method for controllable image generation; In video generation, which involves additional complexity due to motion, recent works have explored methods for motion control. Training-based methods, such as those in [43, 50], allow for trajectory-based motion control, while [19] achieves video control through designed masking in the diffusion process. Unlike these approaches, our method leverages attention maps in a training-free manner for directional motion control. Our model can control the movement of specific objects within the generated video, and uniquely, it enables motion intensity control—providing a new level of flexibility in video generation not addressed in previous works.

## 3. Preliminaries

**Latent Video Diffusion.** Latent Diffusion Models (LDMs), such as Stable Diffusion [34], consist of two main components: an autoencoder and a denoising network. The autoencoder encodes images into a latent space, while the denoising network operates within this latent space, progressively transforming random noise into a coherent image representation. Building on this, Latent Video Diffusion Models (LVDMs) [14] extend LDMs to video generation by incorporating temporal dynamics in the latent space. They are trained using a noise-prediction

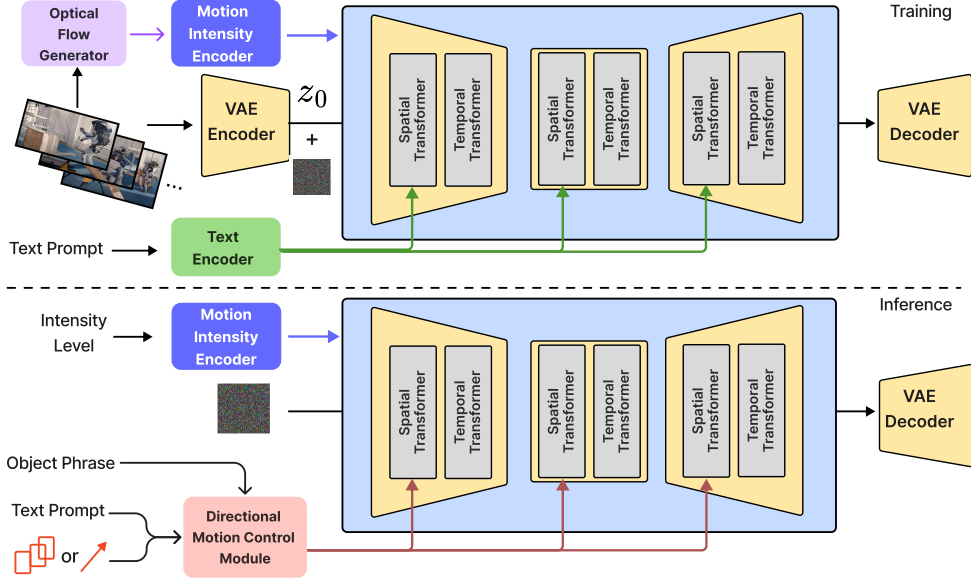


Figure 2. Overview of the Mojito framework. In the training pipeline (top), Mojito uses a VAE Encoder to transform input frames into latent features, processed by Spatial and Temporal Transformers. Motion control is introduced through the Motion Intensity Encoder. During inference (bottom), Mojito generates videos following user-defined motion intensity and directional guidance. The Directional Motion Control Module interprets object phrases within the prompt to align attention with specified trajectories, enabling controlled motion dynamics in the generated video.

objective, minimizing the difference between predicted and actual noise added to the data:

$$\mathcal{L}_{LDM} = \mathbb{E}_i [\|\epsilon - \epsilon_\theta(z_t, t, c)\|_2^2], \quad (1)$$

where  $\epsilon_\theta(\cdot)$  is the noise prediction function of the U-Net, and the condition  $c$  is provided to the U-Net through cross-attention, enabling control based on input text or other conditioning signals. The latent state  $z_t$  follows a Markov process, with Gaussian noise progressively added at each step to the initial latent state  $z_0$ :

$$z_t = \sqrt{\bar{\alpha}_t} z_0 + \sqrt{1 - \bar{\alpha}_t} \epsilon, \quad \epsilon \sim \mathcal{N}(0, I), \quad (2)$$

where  $\bar{\alpha}_t = \prod_{i=1}^t (1 - \beta_i)$  and  $\beta_t$  is a step-dependent coefficient that controls noise strength at time  $t$ .

**Motions in Video Generation.** Motion in videos generally consists of two main components: *direction* and *intensity*. The direction of motion is derived from the trajectory or bounding boxes that an object follows across frames, while the intensity (or strength) reflects the speed and amplitude of movement along this path.

We define a motion trajectory as a sequence of spatial positions:  $\mathcal{T} = \{(x_1, y_1), (x_2, y_2), \dots, (x_L, y_L)\}$ , where each  $(x_i, y_i)$  represents the object’s position in frame  $i$ , with  $x \in [0, W)$  and  $y \in [0, H)$ , where  $L$  is the total number of frames, and  $W$  and  $H$  are the width and height of the video frame, respectively.

## 4. Motion-Controlled Video Generation

Figure 2 illustrates the architecture of Mojito, which comprises two core modules for motion control: the *Directional Motion Control* (DMC) module and the *Motion Intensity Modulator* (MIM) module. These modules work together to allow controlled motion in terms of direction and intensity, as well as to coordinate interaction with the generated video content. We first introduce the test-time, training-free direction control, followed by details on the intensity encoding process. And then we will introduce the motion intensity modulator to modulate the motion intensity and generate videos with the given strength.

### 4.1. Training-Free Directional Motion Control

Existing text-to-video generation models often struggle to achieve user-defined motion direction, such as following a specific trajectory for an object. We address this limitation by introducing a method that dynamically guides motion direction during inference-time sampling, generating samples from a conditional distribution  $p(z|y, \mathcal{T}, i)$  with additional directional controls. Here,  $z$  represents the generated latent video,  $y$  is the input text, and  $\mathcal{T}$  specifies a user-defined input trajectory associated with certain tokens  $y_n$ . This directional control is achieved by modifying attention responses within cross-attention layers in the spatial transformer block of Mojito, as shown in Figure 3.

Cross-attention layers are essential for managing spa-

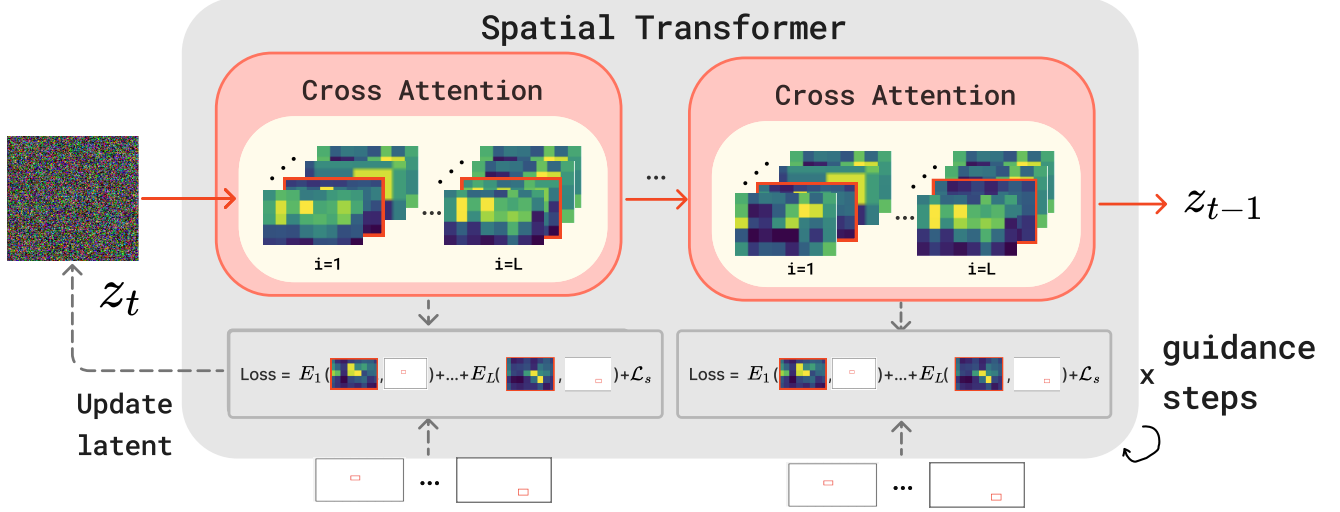


Figure 3. Overview of the directional motion control module. The cross-attention map for the chosen word token in the given guidance step is marked with a red border. We compute the loss and perform backpropagation during inference time to update latents.

---

#### Algorithm 1 Training-Free Directional Motion Control

---

**Require:** Input text  $y$ , object phrase  $y_n$ , user-defined trajectory  $\mathcal{T}$ , denoiser  $D$ , guidance strength  $\eta$ , temporal smoothness weight  $\lambda$ , final guidance timestep  $t_g$

- 1: Initialize latent variable  $z^{(T)} \sim \mathcal{N}(0, I)$
  - 2: **for**  $t = T$  to  $t_g$  **do**
  - 3:    $\sigma_t = \sqrt{\frac{1-\alpha_t}{\alpha_t}}$    # Compute noise level
  - 4:    $A_i^{(\gamma)} = \text{Attention}(y_n, u, i)$    # Compute attention
  - 5:    $B_i = \text{Region}(\mathcal{T}, i)$
  - 6:    $E_i(A_i^{(\gamma)}, B_i, n) = \left(1 - \frac{\sum_{u \in B_i} A_{i,u,n}^{(\gamma)}}{\sum_u A_{i,u,n}^{(\gamma)}}\right)^2$    # Compute energy function for frame  $i$
  - 7:    $\mathcal{L}_s = \mathbb{E}_i[\|A_{i,:}^{(\gamma)} - A_{i-1,:}^{(\gamma)}\|^2]$    # Compute temporal smoothness loss
  - 8:    $G = \nabla_{z^{(t)}} \sum_{i=1}^L \sum_{\gamma \in \Gamma} (E_i(A_i^{(\gamma)}, B_i, n) + \lambda \mathcal{L}_s)$    # Compute gradient
  - 9:    $z^{(t)} \leftarrow z^{(t)} - \sigma_t^2 \eta G$    # Update latent variable
  - 10: **end for**
  - 11: **return** Generated video from  $z^{(0)}$
- 

tial layouts in generated content [7, 11, 15]. The attention score  $A_{u,n}^{(\gamma)}$  between spatial location  $u$ , text token  $y_n$  in cross-attention layer  $\gamma$  determines their association, with  $\sum_{n=1}^N A_{u,n}^{(\gamma)} = 1$ . This competitive interaction among text tokens helps guide object motion by biasing attention maps. By aligning attention focus along the trajectory  $\mathcal{T}$  with the token  $y_n$ , we gain fine-grained frame-by-frame control over object placement without requiring additional training.

Specifically, for a given input trajectory  $\mathcal{T} = \{(x_i, y_i)\}_{i=1}^L$ , where  $L$  is the number of points in the trajectory, we expand each point  $(x_i, y_i)$  to create a bounding box  $B_i$  for frame  $i$ . This bounding box is defined as:

$$B_i = \{(x, y) : |x - x_i| \leq \Delta_x, |y - y_i| \leq \Delta_y\}, \quad (3)$$

where  $\Delta_x$  and  $\Delta_y$  are tolerance values that define the size of the bounding box around each trajectory point. These bounding boxes  $B_i$  are allocated for each video frame  $i$ , ensuring alignment with the trajectory.

To align the attention maps with the bounding boxes over the course of the video, we define a frame-specific energy function  $E_i$  at each video timestep  $i$ :

$$E_i(A_i^{(\gamma)}, B_i, n) = \left(1 - \frac{\sum_{u \in B_i} A_{i,u,n}^{(\gamma)}}{\sum_u A_{i,u,n}^{(\gamma)}}\right)^2, \quad (4)$$

where  $A_{i,u,n}^{(\gamma)}$  denotes the attention score at video timestep  $i$  in layer  $\gamma$ , spatial location  $u$ , and text token  $y_n$ . This function encourages attention to concentrate within the bounding box  $B_i$  at each timestep  $i$ , thereby achieving effective alignment of the attention with the trajectory throughout the video sequence.

**Temporal Smoothness Loss.** To ensure temporal coherence and avoid abrupt changes in motion, we introduce a temporal smoothness loss across frames, defined as the expectation of squared differences in attention maps over consecutive frames:

$$\mathcal{L}_s = \mathbb{E}_i[\|A_{i,:}^{(\gamma)} - A_{i-1,:}^{(\gamma)}\|^2], \quad (5)$$

where  $A_{i,\dots}^{(\gamma)}$  and  $A_{i-1,\dots}^{(\gamma)}$  are attention maps for consecutive frames  $i$  and  $i-1$ . This loss penalizes large frame-to-frame attention changes, promoting smooth motion across frames.

**Gradient Update.** The latent variable  $z^{(t)}$  at diffusion timestep  $t$  is iteratively updated using the gradients of the combined energy functions:

$$z^{(t)} \leftarrow z^{(t)} - \sigma_t^2 \eta \nabla_{z^{(t)}} \sum_{i=1}^L \sum_{\gamma \in \Gamma} \left( E_i \left( A_i^{(\gamma)}, B_i, n \right) + \lambda \mathcal{L}_s \right), \quad (6)$$

where  $\eta > 0$  controls the guidance strength,  $\lambda$  controls the scale of the temporal smoothness loss, and  $\sigma_t = \sqrt{\frac{1-\alpha_t}{\alpha_t}}$  adjusts for the noise level at diffusion timestep  $t$ . Scaling by  $\sigma_t^2$  ensures that early diffusion timesteps with high noise receive weaker guidance, which intensifies as noise decreases in later timesteps, refining latent representations near the end of the diffusion process.

To generate a video, we alternate between gradient updates and denoising steps, iteratively refining the latent variable  $z^{(t)}$  to align cross-attention maps with the intended trajectory. The combination of iterative guidance and smoothness enforcement allows the model to produce coherent video sequences with precise spatial control. The overall algorithm of the DMC module is shown in Algorithm 1.

## 4.2. Motion Intensity Modulator Module

The Motion Intensity Modulator (MIM) module enables controlled adjustment of motion intensity in generated videos. During training, we compute the optical flow [16] strength between consecutive frames to quantify motion intensity, using this information as a conditioning input for the diffusion model. This conditioning allows the model to capture varying levels of motion intensity, guiding the generation process based on the specified motion dynamics.

**Optical Flow Map Generation.** To extract motion intensity from the video, we first generate optical flow maps that visualize the motion dynamics across frames. Optical flow maps provide pixel-wise information on both the direction and magnitude of movement between consecutive frames, enabling a quantifiable representation of motion intensity. For each video, we sequentially read frames and convert them to grayscale, which allows efficient optical flow calculation using the Farneback method [10]. This dense optical flow method computes the motion between frames. From these components, we derive the magnitude, and the magnitude values provide a measure of motion intensity.

**Motion Intensity Encoder.** To incorporate the motion intensity into our model, we convert the optical flow strength of the video into motion embeddings. Similar to [22], rather than feeding the motion intensity as a raw numerical value, we transform it into a word form before training. This aligns with the CLIP model’s preference for text-based representations, as CLIP serves as our text encoder. This approach leverages CLIP’s capability to interpret motion intensity as a semantic feature.

The motion intensity is embedded through a learned embedding layer  $\mathcal{M}$ , which maps the motion intensity to an embedding vector  $c_M$ . This vector is duplicated and concatenated with itself to ensure that its influence is strong enough when combined with the text embeddings.

**Training and Loss Function.** The model is trained by minimizing the following loss function:

$$\mathcal{L}'_{LDM} = \mathbb{E} \left[ \|\epsilon - \epsilon_\theta(z_t, t, c_T, c_M)\|_2^2 \right]. \quad (7)$$

Here,  $c_M$  represents the motion intensity condition and  $c_T$  the text condition, which together provide a comprehensive conditioning signal for guiding the generation of temporally consistent, motion-controlled videos.

**Inference.** During inference, for motion intensity guidance, Mojito takes two inputs: a text prompt, and the motion intensity. These inputs are processed in two pathways: one directly through the diffusion model and the other through the MIM module. The text embedding  $c_T$  is obtained by processing the text prompt via the CLIP text encoder, while the motion embedding  $c_M$  is generated through the motion intensity embedding layer. The final conditioning input  $c_L = c_T + c_M$  combines the text and motion embeddings, allowing the generation process to be guided with both semantic and motion-based conditioning.

## 4.3. Model Backbone

The backbone of Mojito is based on a Conv-Spatial-Temporal Transformer architecture. The model structure consists of input blocks, a mid-block, and output blocks, each containing convolutional layers, temporal transformers, and spatial transformers. This design enables handling motion control in both the temporal and spatial dimensions.

The *Temporal Transformer* processes video data along the time axis, capturing dependencies between frames by reshaping the input into temporal sequences. This block includes relative position encoding and optional causal masking for unidirectional attention, making it effective for capturing motion patterns across frames. Group normalization (GroupNorm) ensures stability in representation learning.

The *Spatial Transformer* captures spatial relationships within each frame. Using linear or convolutional projec-

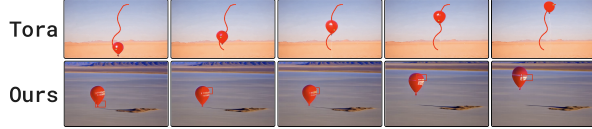


Figure 4. Qualitative comparison of directional control with baselines. Mojito achieves accurate control over object motion by specifying objects and precise locations without requiring additional training. The **red bounding boxes**, serving as inputs to Mojito, guide the generated balloon to follow the specified trajectory.

tions, this block reshapes and processes spatial information to learn localized patterns, which is essential for high-resolution video generation. Cross-attention layers enable alignment with external context when available, further refining spatial coherence in the generated content. The Directional Motion Control module works on this module.

Together, the temporal and spatial transformers enable Mojito to control motion directions and intensities. The details of the model architecture is given in the SUPPLEMENTARY MATERIALS.

## 5. Experiments

### 5.1. Datasets

We use Panda70M [8], InternVID [42], Mira [21] to train the model backbone and the Motion Intensity Modulator module. For Panda-70M, from which we collected a high quality training-10M subset. We processed another 1,000 videos for evaluation purpose for the motion intensity modulator. For motion direction guidance evaluation, we use the LaSOT [9] dataset which contains prompt-bbox-video annotations; For InternVID and Mira, we processed and used the whole dataset for training. The details are given in the Supplementary materials.

### 5.2. Evaluation Metrics

For quantitative evaluation, we employ commonly used metrics: Fréchet Video Distance (FVD) [39] and CLIP-SIM [44], which calculates the average similarity across all generated frames in relation to the input caption. Specifically, we compute the FVD for a set of 300 videos, each consisting of 16 frames.

To quantify the efficacy of direction guidance, we use the off-the-shelf OWL-ViT-large open-vocabulary object detector [25] to detect the bounding box annotations of generated videos. We compute the Intersection-over-Union [33] of the detected bboxes and the input bboxes on videos. We also compute the Centroid Distance (CD) as the distance between the centroid of generated objects and input bboxes, normalized to 1. Finally, we report the average precision@50% (AP50) of the detected and input bboxes; For motion intensity control, we compute the difference be-

tween the detected average optical flow in the generated video and the target motion intensity, normalized to 1.

### 5.3. Implementation Details

**Model backbone.** For the Variational Autoencoder (VAE) framework, the encoder processes input frames at a resolution of  $320 \times 512$ , progressively downsampling through a series of residual blocks and convolutional layers with channel multipliers of (1, 2, 4, 4). This results in a latent representation with a spatial resolution of  $40 \times 64$ . We use CLIP (ViT-H-14) [30] as the text encoder, allowing for high-quality text-to-video alignment. For video processing, spatial and temporal downsampling factors of 8 are applied in both dimensions. The attention matrices (such as  $q$  and  $kv$ ) within the spatial transformer are structured as  $(t, b, c)$ , where  $t$  represents the temporal length. Trajectory adjustments are applied only within the mid-block and the initial layers of the upsampling branch in the denoising U-Net [35], which provides a balance between maintaining video quality and achieving precise motion control. Additional implementation details and parameter settings are provided in the SUPPLEMENTARY MATERIALS.

**Training.** We use the DeepSpeed [32] framework to train our model, utilizing memory and computation optimizations for distributed training. The model training is carried out using the FusedLamb [48] optimizer combined with the LambdaLR Scheduler. We use a batch size of 4 and a base learning rate of  $1.0 \times 10^{-5}$ . More details can be found in the SUPPLEMENTARY MATERIALS.

### 5.4. Performance Evaluation

**Qualitative Comparison on Directional Control** We present a qualitative comparison with Tora [50] in Figure 4. The text prompt used is “A **red helium balloon** floats slowly upward into the sky over a barren desert and expansive Gobi landscape.” The benefits of Mojito are threefold. **First**, Mojito features a *training-free capability*, enabling precise directional control at test time without requiring additional training data or fine-tuning. Unlike training-based approaches like Tora, Mojito can dynamically adjust object trajectories during sampling at inference time, ensuring robust control without added computational cost in training. **Second**, Mojito provides *fine-grained directional control* by allowing users to specify motion paths for named objects. This level of control contrasts with baseline models like Tora, which lack the capability to follow object-specific directional prompts and typically follow arbitrary trajectories. In Figure 4, we showcase scenarios where Mojito is given specific object names (e.g., “red helium balloon”) and precise locations, enabling it to guide each object’s motion along user-defined paths.

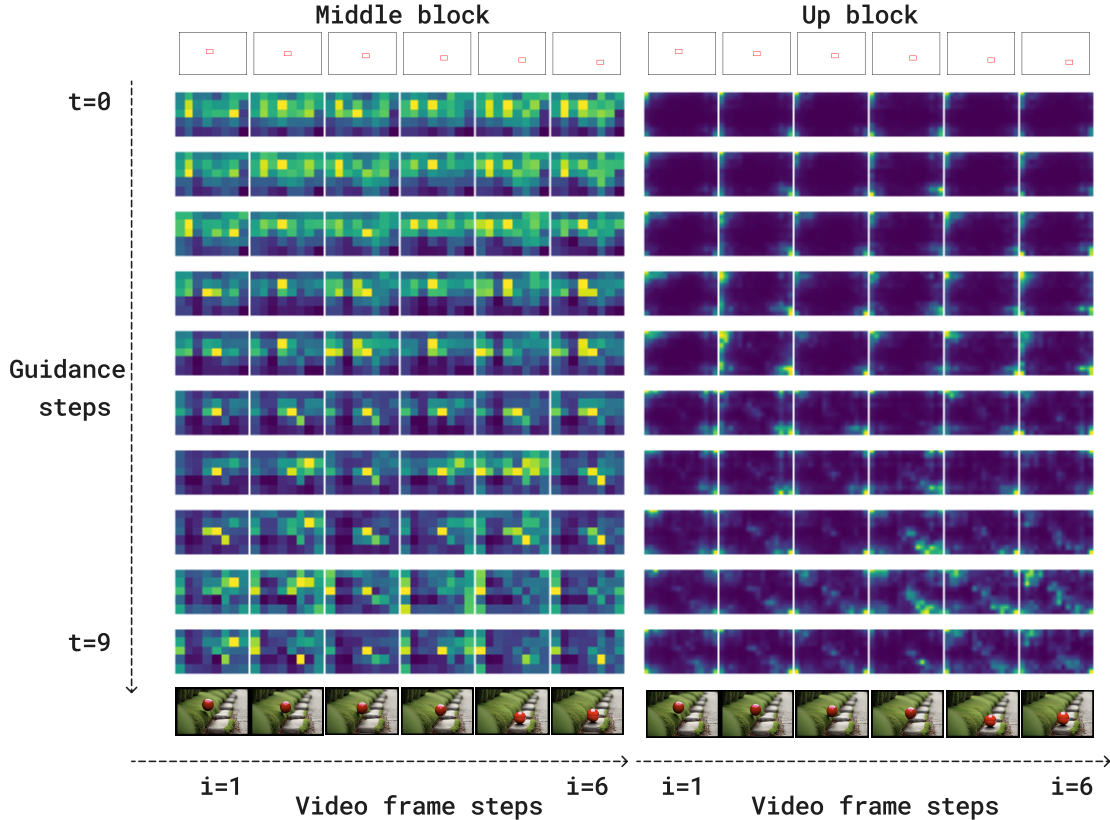


Figure 5. Progression of cross-attention maps during sampling steps for directional guidance. Initially, the attention map for the red ball shows random patterns, but as sampling progresses, it increasingly aligns with the bounding boxes set for each video timestep. (Zoom in for better visualization.)

Table 1. Human evaluation between Mojito, OpenSora [52], OpenSora plan [23], and VideoCrafter2 [5]. It includes 2400 comparisons on 400 video pairs. Each video pair contains 5 ratings from different human annotators on Amazon Turk. The detailed setup is given in the SUPPLEMENTARY MATERIALS.

	Mojito	Tie	OpenSora [52]	Mojito	Tie	VideoCrafter2 [5]	Mojito	Tie	OpenSora plan [23]
Direction Alignment	<b>84.8%</b>	3.3%	12.0%	<b>88.0%</b>	5.0%	7.0%	<b>86.8%</b>	3.0%	10.3%
Intensity Alignment	<b>46.8%</b>	22.3%	31.0%	<b>40.0%</b>	28.5%	31.5%	<b>43.5%</b>	23.8%	32.8%

Table 2. Quantitative evaluation of trajectory alignment and video quality with different total numbers of guidance steps. Setting higher guidance steps generally enhances trajectory alignment while maintaining video quality.

Method	FVD ↓	CLIPSIM ↑	Direction		
			mIoU ↑	AP50 ↑	CD ↓
$t = 1$	423	0.2520	18.0	11.2	0.34
$t = 5$	<b>422</b>	0.2511	24.5	14.4	0.32
$t = 10$	<b>422</b>	<b>0.3700</b>	26.0	17.1	<b>0.28</b>
$t = 30$	479	0.1880	<b>28.3</b>	<b>18.9</b>	<b>0.28</b>

Table 3. Quantitative evaluation of different designs for the Motion Intensity Modulator (MIM). Combining motion intensity embeddings with text embeddings achieves the best overall performance, balancing video quality, semantic similarity, and motion alignment. Treating motion intensity embeddings as a global conditional input shows good motion alignment but significantly degrades video quality

Method	FVD ↓	CLIPSIM ↑	Motion Alignment ↓
w/o MIM	421	0.250	0.307
Global Conditional Input	438	0.250	0.097
Direct Text Input	<b>422</b>	0.256	0.174
Combined with Text Embedding	423	<b>0.273</b>	<b>0.089</b>

**Human Evaluation.** We conduct human evaluations to assess the effectiveness of Mojito in both motion intensity



Figure 6. (a) **Ablation Study on Temporal Smoothness Loss**: Without temporal smoothness loss, the generated sailboat exhibits inconsistencies across frames. (b) **Ablation Study on Guidance Strength**: Adjusting the guidance strength demonstrates a trade-off between video quality and trajectory alignment.

control and directional control. For evaluating the Motion Intensity Modulator, we compare Mojito with baselines by rewriting the text prompts for baselines to explicitly specify the desired intensity level. The results of this evaluation are presented in Table 1. Details on the evaluation and settings are provided in the SUPPLEMENTARY MATERIALS.

## 5.5. Visualization of Attention Maps

To understand the progression of directional control in Mojito, we examine cross-attention maps at different sampling steps within the denoising network. The text prompt is “A small red ball bounces along a cobblestone path lined with greenery.” As shown in Figure 5, the attention maps for the target object (the “red ball”) initially display random patterns at the beginning of the sampling process. However, as sampling steps progress, the attention gradually refines and starts to align with the bounding boxes defined for each video timestep. This refinement ensures that the generated video closely follows the user-defined trajectory.

## 5.6. Ablation Study

### 5.6.1. Directional Control

In this section, we analyze the effects of various configurations for directional control, specifically examining different values of guidance strength ( $\eta$ ), temporal smoothness loss ( $\lambda$ ), and guidance steps. The results are presented in Figure 6. The text prompt used is “A vintage wooden sailboat glides steadily down a mist-covered river.” and “A dolphin leaps through the waves of the ocean at sunrise.”

**Temporal Smoothness Loss.** When  $\lambda = 0$  (no temporal smoothness loss), the generated video exhibits noticeable changes in views and inconsistent sailboat appearances.

**Guidance Strength.** With  $\eta = 0$  (no guidance strength), the generated “sailboat” does not follow specified bounding boxes at all. As  $\eta$  increases, the sailboat begins to follow bounding boxes more closely. The best results reaches with  $\eta = 100$ , where the sailboat’s trajectory aligns well with the bounding boxes while maintaining good visual quality. However, setting  $\eta$  to an excessively high value



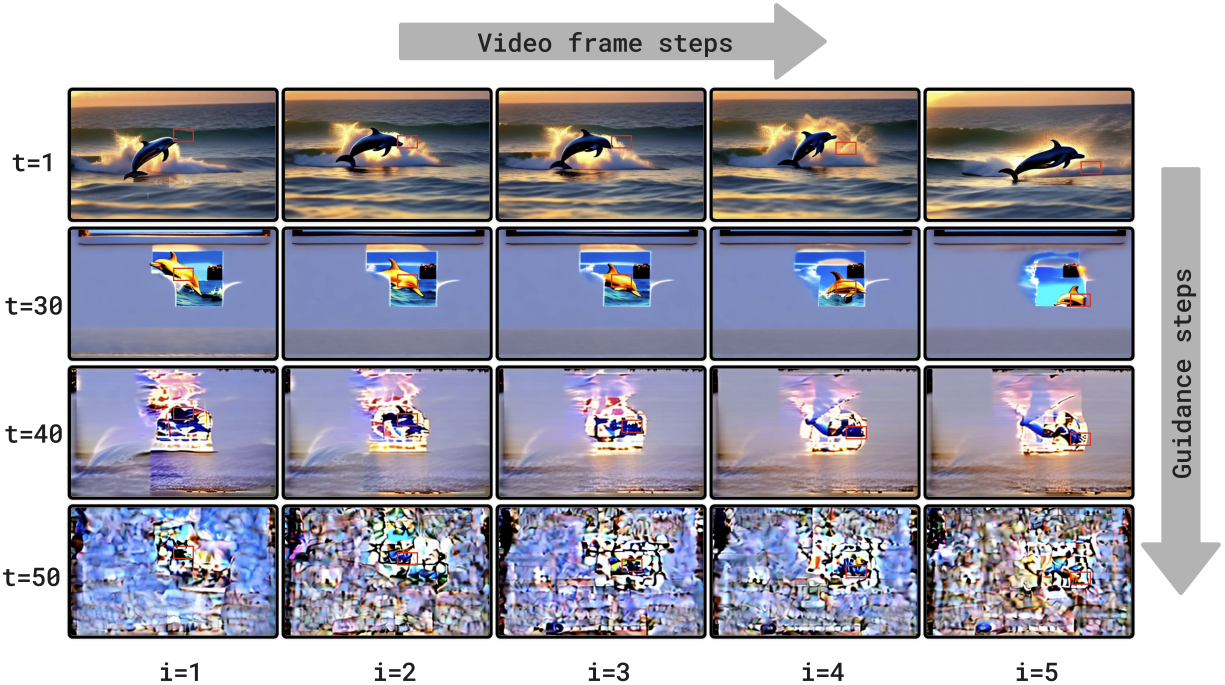


Figure 7. Ablation study on the effect of guidance steps. While increasing the number of guidance steps improves trajectory alignment, excessive guidance steps can degrade overall video quality.

(e.g.,  $\eta = 10000$ ) results in severe degradation of video quality, with visible artifacts such as square patterns.

**Guidance Steps.** We perform an additional experiment to evaluate the effect of varying the number of guidance steps on video quality and trajectory alignment. The results, shown in Table 2, indicate that increasing the number of guidance steps from  $t = 1$  to  $t = 10$  generally enhances trajectory alignment without significantly impacting video quality. However, when the number of guidance steps becomes too large (e.g.,  $t \geq 30$ ), the video quality deteriorates substantially. Qualitative results illustrating this effect are provided in Figure 7.

### 5.6.2. Motion Intensity Modulator

In this section, we explore various designs for the Motion Intensity Modulator (MIM). The primary approach in this paper involves combining a motion intensity embedding with text prompt embeddings and feeding them into Mojito. Additionally, we experimented with several alternatives:

**Without MIM.** Removing the MIM module during training and testing. In this setup, we perform inference by rewriting the text prompts to include the intensity level.

**Global Conditional Input.** Combining the intensity embedding with FPS and time embeddings, using this global embedding as a conditioning input for convolution layers.

**Direct Text Input with Fine-tuning.** In this approach, we rewrite the text prompts to include the motion intensity level and then fine-tune the model using this new data. Both training and inference are guided by the modified text input that explicitly specifies the motion intensity.

To compare each design, we evaluated the alignment of optical flow between the generated and input videos, as well as video quality and semantic similarity metrics. The quantitative results for each design are shown in Table 3, indicate that combining motion intensity embeddings with text embeddings yields the best performance. This demonstrates that treating motion intensity as an additional conditioning input and incorporating it into the cross-attention alongside text embeddings is a highly effective strategy.

## 6. Conclusion

In this work, we presented Mojito, a novel framework for text-to-video generation that enables precise control over motion direction and intensity. By introducing the Di-

rectional Motion Control module and the Motion Intensity Modulator module, Mojito allows to specify object trajectories and motion intensity, enhancing flexibility in video generation. Experiments demonstrate Mojito’s effectiveness and efficiency in producing high-quality, motion-controlled videos with minimal reliance on additional annotated videos.

## References

- [1] Andreas Blattmann, Tim Dockhorn, Sumith Kulal, Daniel Mendelevitch, Maciej Kilian, Dominik Lorenz, Yam Levi, Zion English, Vikram Voleti, Adam Letts, Varun Jampani, and Robin Rombach. Stable video diffusion: Scaling latent video diffusion models to large datasets. *NONE*, 2023. 1
- [2] Andreas Blattmann, Robin Rombach, Huan Ling, Tim Dockhorn, Seung Wook Kim, Sanja Fidler, and Karsten Kreis. Align your latents: High-resolution video synthesis with latent diffusion models. *CVPR*, 2023. 2
- [3] Huiwen Chang, Han Zhang, Jarred Barber, AJ Maschinot, Jose Lezama, Lu Jiang, Ming-Hsuan Yang, Kevin Murphy, William T Freeman, Michael Rubinstein, et al. Muse: Text-to-image generation via masked generative transformers. *arXiv preprint arXiv:2301.00704*, 2023. 1
- [4] Hila Chefer, Yuval Alaluf, Yael Vinker, Lior Wolf, and Daniel Cohen-Or. Attend-and-excite: Attention-based semantic guidance for text-to-image diffusion models. *ACM Transactions on Graphics (TOG)*, 42(4):1–10, 2023. 2
- [5] Haoxin Chen, Yong Zhang, Xiaodong Cun, Menghan Xia, Xintao Wang, Chao Weng, and Ying Shan. Videocrafter2: Overcoming data limitations for high-quality video diffusion models, 2024. 2, 7
- [6] Minghao Chen, Iro Laina, and Andrea Vedaldi. Training-free layout control with cross-attention guidance. *arXiv preprint arXiv:2304.03373*, 2023. 2
- [7] Minghao Chen, Iro Laina, and Andrea Vedaldi. Training-free layout control with cross-attention guidance. In *Proceedings of the IEEE/CVF Winter Conference on Applications of Computer Vision*, pages 5343–5353, 2024. 4
- [8] Tsai-Shien Chen, Aliaksandr Siarohin, Willi Menapace, Ekaterina Deyneka, Hsiang-wei Chao, Byung Eun Jeon, Yuwei Fang, Hsin-Ying Lee, Jian Ren, Ming-Hsuan Yang, et al. Panda-70m: Captioning 70m videos with multiple cross-modality teachers. In *Proceedings of the IEEE/CVF Conference on Computer Vision and Pattern Recognition*, pages 13320–13331, 2024. 6, 1
- [9] Heng Fan, Hexin Bai, Liting Lin, Fan Yang, Peng Chu, Ge Deng, Sijia Yu, Harshit, Mingzhen Huang, Juehuan Liu, et al. Lasot: A high-quality large-scale single object tracking benchmark. *International Journal of Computer Vision*, 129: 439–461, 2021. 6
- [10] Gunnar Farneback. Two-frame motion estimation based on polynomial expansion. In *Image Analysis: 13th Scandinavian Conference, SCIA 2003 Halmstad, Sweden, June 29–July 2, 2003 Proceedings 13*, pages 363–370. Springer, 2003. 5
- [11] Weixi Feng, Xuehai He, Tsu-Jui Fu, Varun Jampani, Arjun Akula, Pradyumna Narayana, Sugato Basu, Xin Eric Wang, and William Yang Wang. Training-free structured diffusion guidance for compositional text-to-image synthesis. *arXiv preprint arXiv:2212.05032*, 2022. 2, 4
- [12] Rohit Girdhar, Alaaeldin El-Nouby, Zhuang Liu, Mannat Singh, Kalyan Vasudev Alwala, Armand Joulin, and Ishan Misra. Imagebind: One embedding space to bind them all. In *Proceedings of the IEEE/CVF Conference on Computer Vision and Pattern Recognition*, pages 15180–15190, 2023. 1
- [13] Xuehai He, Jian Zheng, Jacob Zhiyuan Fang, Robinson Piramuthu, Mohit Bansal, Vicente Ordonez, Gunnar A Sigurdsson, Nanyun Peng, and Xin Eric Wang. Flexecontrol: Flexible and efficient multimodal control for text-to-image generation. *arXiv preprint arXiv:2405.04834*, 2024. 2
- [14] Yingqing He, Tianyu Yang, Yong Zhang, Ying Shan, and Qifeng Chen. Latent video diffusion models for high-fidelity long video generation. *arXiv preprint arXiv: 2211.13221*, 2022. 1, 2
- [15] Amir Hertz, Ron Mokady, Jay Tenenbaum, Kfir Aberman, Yael Pritch, and Daniel Cohen-Or. Prompt-to-prompt image editing with cross attention control. *arXiv preprint arXiv:2208.01626*, 2022. 4
- [16] Berthold KP Horn and Brian G Schunck. Determining optical flow. *Artificial intelligence*, 17(1-3):185–203, 1981. 5
- [17] Lianghua Huang, Di Chen, Yu Liu, Yujun Shen, Deli Zhao, and Jingren Zhou. Composer: Creative and controllable image synthesis with composable conditions. *arXiv preprint arXiv:2302.09778*, 2023. 2
- [18] Gabriel Ilharco, Mitchell Wortsman, Ross Wightman, Cade Gordon, Nicholas Carlini, Rohan Taori, Achal Dave, Vaishaal Shankar, Hongseok Namkoong, John Miller, Hannaneh Hajishirzi, Ali Farhadi, and Ludwig Schmidt. Openclip, 2021. If you use this software, please cite it as below. 1
- [19] Yash Jain, Anshul Nasery, Vibhav Vineet, and Harkirat Behl. Peekaboo: Interactive video generation via masked-diffusion. In *Proceedings of the IEEE/CVF Conference on Computer Vision and Pattern Recognition*, pages 8079–8088, 2024. 2
- [20] Kenan Jiang, Xuehai He, Ruize Xu, and Xin Eric Wang. Comclip: Training-free compositional image and text matching. *arXiv preprint arXiv:2211.13854*, 2022. 1
- [21] Xuan Ju, Yiming Gao, Zhaoyang Zhang, Ziyang Yuan, Xintao Wang, Ailing Zeng, Yu Xiong, Qiang Xu, and Ying Shan. Miradata: A large-scale video dataset with long durations and structured captions. *arXiv preprint arXiv:2407.06358*, 2024. 6, 1
- [22] Hitesh Kandala, Jianfeng Gao, and Jianwei Yang. Pix2gif: Motion-guided diffusion for gif generation. *arXiv preprint arXiv:2403.04634*, 2024. 5
- [23] PKU-Yuan Lab and Tuzhan AI etc. Open-sora-plan, 2024. 1, 2, 7
- [24] Yuheng Li, Haotian Liu, Qingyang Wu, Fangzhou Mu, Jianwei Yang, Jianfeng Gao, Chunyuan Li, and Yong Jae Lee. Gligen: Open-set grounded text-to-image generation. *2023 IEEE/CVF Conference on Computer Vision and Pattern Recognition (CVPR)*, 2023. 2

- [25] Matthias Minderer, Alexey Gritsenko, Austin Stone, Maxim Neumann, Dirk Weissenborn, Alexey Dosovitskiy, Aravindh Mahendran, Anurag Arnab, Mostafa Dehghani, Zhuoran Shen, et al. Simple open-vocabulary object detection. In *European Conference on Computer Vision*, pages 728–755. Springer, 2022. 6
- [26] Sicheng Mo, Fangzhou Mu, Kuan Heng Lin, Yanli Liu, Bochen Guan, Yin Li, and Bolei Zhou. Freecontrol: Training-free spatial control of any text-to-image diffusion model with any condition. In *Proceedings of the IEEE/CVF Conference on Computer Vision and Pattern Recognition*, pages 7465–7475, 2024. 2
- [27] Chong Mou, Xintao Wang, Liangbin Xie, Jian Zhang, Zhonggang Qi, Ying Shan, and Xiaohe Qie. T2i-adapter: Learning adapters to dig out more controllable ability for text-to-image diffusion models. *arXiv preprint arXiv:2302.08453*, 2023. 2
- [28] Alexander Quinn Nichol, Prafulla Dhariwal, Aditya Ramesh, Pranav Shyam, Pamela Mishkin, Bob McGrew, Ilya Sutskever, and Mark Chen. Glide: Towards photorealistic image generation and editing with text-guided diffusion models. *arXiv preprint arXiv:2112.10741*, 2021. 1
- [29] Can Qin, Shu Zhang, Ning Yu, Yihao Feng, Xinyi Yang, Yingbo Zhou, Huan Wang, Juan Carlos Niebles, Caiming Xiong, Silvio Savarese, et al. Unicontrol: A unified diffusion model for controllable visual generation in the wild. *arXiv preprint arXiv:2305.11147*, 2023. 2
- [30] Alec Radford, Jong Wook Kim, Chris Hallacy, Aditya Ramesh, Gabriel Goh, Sandhini Agarwal, Girish Sastry, Amanda Askell, Pamela Mishkin, Jack Clark, et al. Learning transferable visual models from natural language supervision. *arXiv preprint arXiv:2103.00020*, 2021. 6
- [31] Aditya Ramesh, Mikhail Pavlov, Gabriel Goh, Scott Gray, Chelsea Voss, Alec Radford, Mark Chen, and Ilya Sutskever. Zero-shot text-to-image generation. In *International Conference on Machine Learning*, pages 8821–8831. PMLR, 2021. 1
- [32] Jeff Rasley, Samyam Rajbhandari, Olatunji Ruwase, and Yuxiong He. Deepspeed: System optimizations enable training deep learning models with over 100 billion parameters. In *Proceedings of the 26th ACM SIGKDD International Conference on Knowledge Discovery & Data Mining*, page 3505–3506, New York, NY, USA, 2020. Association for Computing Machinery. 6
- [33] Hamid Rezaatfighi, Nathan Tsoi, JunYoung Gwak, Amir Sadeghian, Ian Reid, and Silvio Savarese. Generalized intersection over union: A metric and a loss for bounding box regression. In *Proceedings of the IEEE/CVF conference on computer vision and pattern recognition*, pages 658–666, 2019. 6
- [34] Robin Rombach, Andreas Blattmann, Dominik Lorenz, Patrick Esser, and Björn Ommer. High-resolution image synthesis with latent diffusion models. In *Proceedings of the IEEE/CVF Conference on Computer Vision and Pattern Recognition*, pages 10684–10695, 2022. 1, 2
- [35] Olaf Ronneberger, Philipp Fischer, and Thomas Brox. U-net: Convolutional networks for biomedical image segmentation. In *Medical image computing and computer-assisted intervention—MICCAI 2015: 18th international conference, Munich, Germany, October 5–9, 2015, proceedings, part III 18*, pages 234–241. Springer, 2015. 6
- [36] Chitwan Saharia, William Chan, Saurabh Saxena, Lala Li, Jay Whang, Emily Denton, Seyed Kamyar Seyed Ghasemipour, Burcu Karagol Ayan, S. Sara Mahdavi, Rapha Gontijo Lopes, Tim Salimans, Jonathan Ho, David J Fleet, and Mohammad Norouzi. Photorealistic text-to-image diffusion models with deep language understanding. *arXiv:2205.11487*, 2022. 2
- [37] Chitwan Saharia, William Chan, Saurabh Saxena, Lala Li, Jay Whang, Emily L Denton, Kamyar Ghasemipour, Raphael Gontijo Lopes, Burcu Karagol Ayan, Tim Salimans, et al. Photorealistic text-to-image diffusion models with deep language understanding. *Advances in Neural Information Processing Systems*, 35:36479–36494, 2022. 1
- [38] Uriel Singer, Adam Polyak, Thomas Hayes, Xi Yin, Jie An, Songyang Zhang, Qiyuan Hu, Harry Yang, Oron Ashual, Oran Gafni, Devi Parikh, Sonal Gupta, and Yaniv Taigman. Make-a-video: Text-to-video generation without text-video data. *arXiv preprint arXiv: 2209.14792*, 2022. 2
- [39] Thomas Unterthiner, Sjoerd van Steenkiste, Karol Kurach, Raphaël Marinier, Marcin Michalski, and Sylvain Gelly. Fvd: A new metric for video generation. 2019. 6
- [40] Vchitect. Vchitect 2.0. <https://github.com/Vchitect/Vchitect-2.0>, 2024. Version 2.0, Accessed: 2024-11-09. 1, 2
- [41] Jiuniu Wang, Hangjie Yuan, Dayou Chen, Yingya Zhang, Xiang Wang, and Shiwei Zhang. Modelscope text-to-video technical report. *arXiv preprint arXiv: 2308.06571*, 2023. 2
- [42] Yi Wang, Yanan He, Yizhuo Li, Kunchang Li, Jiashuo Yu, X. Ma, Xinyuan Chen, Yaohui Wang, Ping Luo, Ziwei Liu, Yali Wang, Limin Wang, and Y. Qiao. Internvid: A large-scale video-text dataset for multimodal understanding and generation. *International Conference on Learning Representations*, 2023. 6, 1
- [43] Zhouxia Wang, Ziyang Yuan, Xintao Wang, Yaowei Li, Tianshui Chen, Menghan Xia, Ping Luo, and Ying Shan. Motionctrl: A unified and flexible motion controller for video generation. In *ACM SIGGRAPH 2024 Conference Papers*, pages 1–11, 2024. 2
- [44] Jinbo Xing, Menghan Xia, Yong Zhang, Haoxin Chen, Wangbo Yu, Hanyuan Liu, Gongye Liu, Xintao Wang, Ying Shan, and Tien-Tsin Wong. Dynamicrafter: Animating open-domain images with video diffusion priors. In *European Conference on Computer Vision*, pages 399–417. Springer, 2025. 6
- [45] Jiaqi Xu, Xinyi Zou, Kunzhe Huang, Yunkuo Chen, Bo Liu, MengLi Cheng, Xing Shi, and Jun Huang. Easyanimate: A high-performance long video generation method based on transformer architecture. *arXiv preprint arXiv:2405.18991*, 2024. 1, 2
- [46] Zhengyuan Yang, Jianfeng Wang, Zhe Gan, Linjie Li, Kevin Lin, Chenfei Wu, Nan Duan, Zicheng Liu, Ce Liu, Michael Zeng, et al. Reco: Region-controlled text-to-image generation. In *Proceedings of the IEEE/CVF Conference on Computer Vision and Pattern Recognition*, pages 14246–14255, 2023. 2

- [47] Zhuoyi Yang, Jiayan Teng, Wendi Zheng, Ming Ding, Shiyu Huang, Jiazheng Xu, Yuanming Yang, Wenyi Hong, Xiaohan Zhang, Guanyu Feng, et al. Cogvideox: Text-to-video diffusion models with an expert transformer. *arXiv preprint arXiv:2408.06072*, 2024. [1](#), [2](#)
- [48] Yang You, Jing Li, Sashank Reddi, Jonathan Hseu, Sanjiv Kumar, Srinadh Bhojanapalli, Xiaodan Song, James Demmel, Kurt Keutzer, and Cho-Jui Hsieh. Large batch optimization for deep learning: Training bert in 76 minutes. *arXiv preprint arXiv:1904.00962*, 2019. [6](#)
- [49] Jiahui Yu, Yuanzhong Xu, Jing Yu Koh, Thang Luong, Gungjan Baid, Zirui Wang, Vijay Vasudevan, Alexander Ku, Yinfei Yang, Burcu Karagol Ayan, et al. Scaling autoregressive models for content-rich text-to-image generation. *arXiv preprint arXiv:2206.10789*, 2(3):5, 2022. [1](#)
- [50] Zhenghao Zhang, Junchao Liao, Menghao Li, Long Qin, and Weizhi Wang. Tora: Trajectory-oriented diffusion transformer for video generation. *arXiv preprint arXiv:2407.21705*, 2024. [2](#), [6](#)
- [51] Shihao Zhao, Dongdong Chen, Yen-Chun Chen, Jianmin Bao, Shaozhe Hao, Lu Yuan, and Kwan-Yee K Wong. Uni-controlnet: All-in-one control to text-to-image diffusion models. *arXiv preprint arXiv:2305.16322*, 2023. [2](#)
- [52] Zangwei Zheng, Xiangyu Peng, Tianji Yang, Chenhui Shen, Shenggui Li, Hongxin Liu, Yukun Zhou, Tianyi Li, and Yang You. Open-sora: Democratizing efficient video production for all, 2024. [1](#), [2](#), [7](#)

# Mojito: Motion Trajectory and Intensity Control for Video Generation

## Supplementary Material

### 7. Model Architecture

We illustrate the architecture of Mojito in Figure 8. The model builds upon a VAE-based latent diffusion framework and incorporates both spatial and temporal transformers to achieve fine-grained control over motion direction and intensity. Spatial transformers process spatial information within each frame, while temporal transformers ensure temporal coherence across video frames.

Motion intensity embeddings and text prompt embeddings are integrated into the cross-attention layers, enabling the model to conditionally generate videos based on user-specified motion properties. Additional convolutional layers handle the temporal features like frame per second (fps) and timesteps (t), enhancing the flexibility of the model to adapt to diverse inputs.

### 8. Dataset

We use Panda 70M [8], InternVID [42], and Mira [21] datasets to train Mojito for motion intensity control. For InternVID and Mira, we follow the official data processing setups.

For Panda 70M, we process the data in two stages to ensure semantic consistency and quality. In the first stage, we split long videos using PySceneDetect with a content detector and a cut-scene threshold of 25 frames, introducing artificial cuts every 5 seconds for long, uncut footage. To filter clips with semantic transitions, we compute ImageBind [12] features at 10% and 90% of each clip and retain only those with a Euclidean distance  $\leq 1.0$ .

In the second stage, consecutive clips with similar semantic content are merged by comparing their boundary features and concatenating those with a feature distance  $\leq 0.6$ . Additional post-processing ensures clip quality and diversity: clips shorter than 2 seconds or containing minimal motion are excluded, and clips longer than 60 seconds are trimmed. We further filter clips to ensure semantic diversity (feature distance  $> 0.3$ ) and remove unstable segments by trimming the first and last 10% of each clip. This results in 70,817,169 clips with an average duration of 8.5 seconds.

### 9. Implementation Details

#### 9.1. Training Details

We train our model using a transformer-based diffusion framework. The training process incorporates a combination of spatial and temporal transformers to ensure both spatial coherence and motion control across video frames. Key

training configurations are detailed below:

#### 9.1.1. Training Configuration

The model uses a learning rate of  $1 \times 10^{-3}$  without scaling and is optimized with a step-based LambdaLR scheduler. The scheduler initiates a linear decay of the learning rate from the first training step, targeting a final decay ratio of 0.01 over 20,000 steps. Gradient clipping is applied with a maximum norm of 0.5. Mixed precision training is employed to improve efficiency, with DeepSpeed stage-2 optimization enabled for memory management.

#### 9.1.2. Model Architecture

The autoencoder processes input frames at a resolution of  $320 \times 512$ , downsampling them into a latent space with a spatial resolution of  $40 \times 64$  and a channel depth of 4. The conditional input is encoded using a FrozenOpenCLIPEmbedder [18], which remains fixed during training to leverage text prompts effectively [20]. The model also integrates additional conditioning inputs, such as FPS information, to improve motion control.

#### 9.1.3. Motion Conditioning and Loss Function

Motion intensity control is achieved by introducing optical flow-based motion embeddings as additional conditions. The motion embeddings are combined with text embeddings and fed into cross-attention layers. The diffusion process optimizes a noise-prediction objective:

$$\mathcal{L} = \|\epsilon - \epsilon_\theta(z_t, t, c)\|_2^2, \quad (8)$$

where  $\epsilon_\theta$  predicts the added noise, and  $c$  represents the combined text and motion intensity conditions.

#### 9.1.4. Training Strategy

The model is trained for a maximum of 5,000,000 steps with a batch size of 1 and gradient accumulation over 2 steps. Logging occurs every 50 steps, and checkpoints are saved every 1,000 steps, with additional periodic saving every 5,000 steps. Callback functions log intermediate outputs to monitor the training process.

We utilize PyTorch Lightning for distributed training with DeepSpeed Stage-2 optimization. The training is benchmarked for efficiency, using 32-bit precision for stability. Memory optimizations include overlapping communication and computation, ensuring efficient usage of GPU resources.

### 10. Human Evaluation Interface

In Figure 9, we present the human evaluation interface used on Amazon Mechanical Turk for assessing motion intensity.

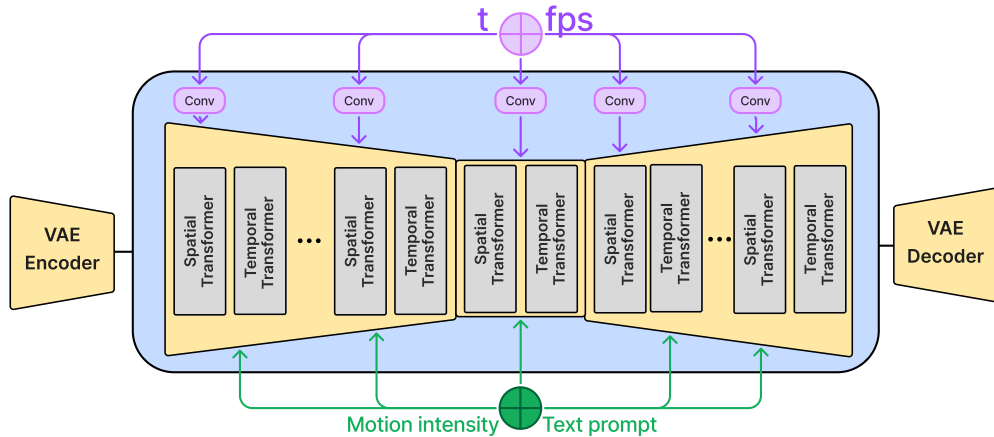
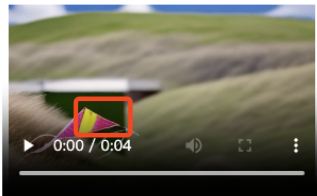


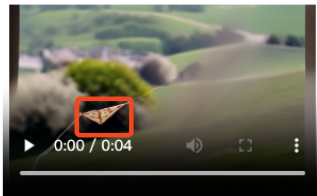
Figure 8. The architecture of Mojito. The framework combines a VAE Encoder-Decoder structure with spatial and temporal transformers to process spatial and temporal information effectively. Motion intensity embeddings and text prompt embeddings condition the cross-attention layers, providing flexible and controllable motion direction and strength. Temporal convolutional layers handle features like frame per second (fps) and timesteps (t), allowing the model to generate temporally coherent and spatially consistent videos.

**Input Prompt:** A small kite flies high above a grassy hill on a windy day.

**Video A**



**Video B**



1. Carefully watch both videos provided and review the input prompt.
2. Carefully review the input bounding boxes, which describe the expected movement trajectory of the object in the video.
3. Compare how closely the object's movement in each video aligns with the trajectory defined by the input bounding boxes (e.g., staying within the specified path or area).
4. Select the video (Video A or Video B) that better follows the specified trajectory.

Video A

Figure 9. Human evaluation interface for assessing motion direction using Amazon Turkers.

Participants are asked to rate the perceived motion intensity in the generated videos on a predefined scale.

In Figure 10, we display the human evaluation interface used for evaluating motion direction alignment. Participants are instructed to assess how well the motion direction in the videos aligns with the specified trajectories.

## 11. Ablation Study on Guidance Layers

In this section, we conduct an ablation study to evaluate the effect of applying backward guidance on which layers

during the directional motion guidance process. The results are summarized in Table 4.

We apply backward guidance to the cross-attention maps across layers in the down-sampling branch, the mid-block, and the up-sampling branch. Layers in the down-sampling branch (Down-1, Down-2, Down-3) are observed to be less effective for precise trajectory alignment compared to other layers, as they process lower-resolution features that are less sensitive to fine-grained motion details. Conversely, high-resolution layers such as Up-3 provide better trajectory alignment but at the expense of video quality due to

**Input Prompt:** A soccer ball rolls across a grassy field towards the goal.

**Motion Strength Level:** 4 (0: No Motion, 10: Very Large Motion - maximum possible dynamic movement, such as rapid, large-scale changes or highly dynamic actions)

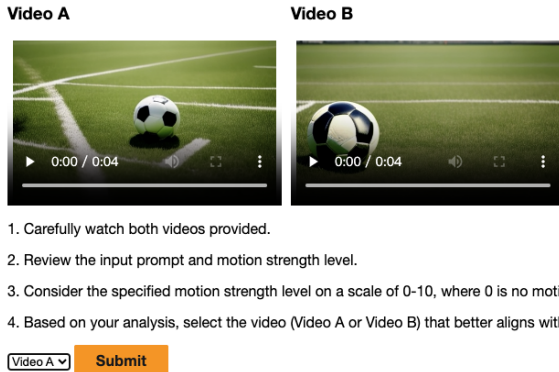


Figure 10. Human evaluation interface for assessing motion intensity using Amazon Turkers.

Table 4. Ablation study on the impact of applying backward guidance on different layers of the U-Net. The best results in terms of trajectory alignment and video quality are achieved by applying guidance to the mid-block (Mid-1) and the first up-sampling layer (Up-1).

Guidance Layers				Metrics		
Down-1	Down-2	Mid-1	Up-1	FVD ↓	mIoU ↑	AP50 ↑
✓				431	18.1	10.9
	✓			428	20.5	12.8
		✓		425	23.8	15.0
			✓	423	24.5	16.2
		✓	✓	<b>422</b>	<b>26.0</b>	<b>17.1</b>
			✓	426	24.0	16.5
		✓		427	22.5	14.7

overfitting to layout constraints. The optimal combination is achieved by applying guidance on the mid-block (Mid-1) and the first up-sampling layer (Up-1), balancing both video quality and trajectory alignment.

## 12. Failure Cases

Figure 11 illustrates two common failure cases observed in directional motion control. The first case occurs when the bounding boxes move significantly faster than the video frame rate. In such situations, multiple objects may appear simultaneously, causing confusion. For example, instead of the first “yellow taxi” moving into the bounding box as intended, a second yellow taxi may appear at the later bounding box location.

The second failure case arises when the text prompt contains similar objects, such as a “sunflower” and a “sun.” In these instances, the guidance mechanism may mistakenly switch focus to the wrong object, resulting in unintended

transitions, such as directing attention from the sunflower to the sun.



A **yellow taxi** drives through a bustling city street, passing people and traffic lights.



A serene wide-angle shot captures a **sunflower** gently swaying in the breeze, set against the backdrop of an expansive golden wheat field under the setting sun.

Figure 11. Failure cases for directional motion control.